Nonlinear properties of AlGaAs waveguides in continuous wave operation regime

C. Lacava,[1,*] V. Pusino,[2] P. Minzioni,[1] M. Sorel,[2] and I. Cristiani[1]

[1]*Dept. of Electrical, Computer, and Biomedical Engineering, Università di Pavia, Via Ferrata, 5 A, 27100 Pavia, Italy*

[2]*School of Engineering, University of Glasgow, UKG12 8LT Glasgow, UK*

[*]*cosimo.lacava@unipv.it*

Abstract: Aluminum Gallium Arsenide (AlGaAs) is an attractive platform for the development of integrated optical circuits for all-optical signal processing thanks to its large nonlinear coefficients in the 1.55-μm telecommunication spectral region. In this paper we discuss the results of the nonlinear continuous-wave optical characterization of AlGaAs waveguides at a wavelength of 1.55 μm. We also report the highest value ever reported in the literature for the real part of the nonlinear coefficient in this material (Re(γ) ≈521 $W^{-1}m^{-1}$).

OCIS codes: (130.0130) Integrated optics; (130.4310) Nonlinear; (190.4380) Nonlinear optics, four-wave mixing.

References and links

1. B. Jalali and F. Sasan, "Silicon photonics," J. Lightwave Technol. **24**(12), 4600–4615 (2006).
2. H. K. Tsang and Y. Liu, "Nonlinear optical properties of silicon waveguides," Semicond. Sci. Technol. **23**(6), 064007 (2008).
3. J. U. Kang, G. I. Stegeman, and J. S. Aitchison, "One-dimensional spatial soliton dragging, trapping, and all-optical switching in AlGaAs waveguides," Opt. Lett. **21**(3), 189–191 (1996).
4. J. S. Aitchison, D. C. Hutchings, J. U. Kang, G. I. Stegeman, and A. Villeneuve, "The nonlinear optical properties of AlGaAs at the half band gap," IEEE J. Quantum Electron. **33**(3), 341–348 (1997).
5. K. Dolgaleva, W. C. Ng, L. Qian, and J. S. Aitchison, "Compact highly-nonlinear AlGaAs waveguides for efficient wavelength conversion," Opt. Express **19**(13), 12440–12455 (2011).
6. J. J. Wathen, P. Apiratikul, B. M. Cannon, T. Mahmood, W. Astar, C. J. K. Richardson, G. Porkolab, G. M. Carter, and T. E. Murphy, "Efficient Continuous-Wave Four-Wave Mixing and Self-Phase Modulation in a Bandgap-Engineered AlGaAs Waveguide,"in Conf. Lasers Electro-Optics 2012 of OSA Technical Digest (Optical Society of America, 2012), paper CW1A.4 (2012).
7. W. Astar, P. Apiratikul, B. M. Cannon, T. Mahmood, J. J. Wathen, J. V. Hryniewicz, S. Kanakaraju, C. J. K. Richardson, T. E. Murphy, and G. M. Carter, "Conversion of RZ-OOK to RZ-BPSK by XPM in a Passive AlGaAs Waveguide," IEEE Photon. Technol. Lett. **23**(19), 1397–1399 (2011).
8. K. Dolgaleva, W. C. Ng, L. Qian, J. S. Aitchison, M. C. Camasta, and M. Sorel, "Broadband self-phase modulation, cross-phase modulation, and four-wave mixing in 9-mm-long AlGaAs waveguides," Opt. Lett. **35**(24), 4093–4095 (2010).
9. D. Duchesne, R. Morandotti, G. A. Siviloglou, G. El, G. I. Stegeman, D. N. Christodoulides, D. Modotto, A. Locatelli, C. De Angelis, F. Pozzi, and M. Sorel, "Nonlinear photonics in AlGaAs photonics nanowires: self phase and cross phase modulation," in Proceedings of International Symposium on Signals, Systems and Electronics, 2007. ISSSE '07 475–478 (2007).
10. G. A. Siviloglou, S. Suntsov, R. El-Ganainy, R. Iwanow, G. I. Stegeman, D. N. Christodoulides, R. Morandotti, D. Modotto, A. Locatelli, C. De Angelis, F. Pozzi, C. R. Stanley, and M. Sorel, "Enhanced third-order nonlinear effects in optical AlGaAs nanowires," Opt. Express **14**(20), 9377–9384 (2006).
11. C. Lee, M. Wu, G. S. Lih, P. L. Fan, and H. Jui-Ming, "Design and analysis of completely adiabatic tapered waveguides by conformal mapping," J. Lightwave Technol. **15**(2), 403–410 (1997).
12. S. J. Pearton, U. K. Chakrabarti, W. S. Hobson, and A. P. Kinsella, "Reactive ion etching of GaAs, AlGaAs, and GaSb in Cl2 and SiCl4," J. Vac. Sci. Technol. B Microelectron. Nanom. Struct. **8**, 607–617 (1990).
13. T. Barwicz and H. A. Haus, "Three-dimensional analysis of scattering losses due to sidewall roughness in microphotonic waveguides," J. Lightwave Technol. **23**(9), 2719–2732 (2005).
14. L. Caspani, D. Duchesne, K. Dolgaleva, S. J. Wagner, M. Ferrera, L. Razzari, A. Pasquazi, M. Peccianti, D. J. Moss, J. S. Aitchison, and R. Morandotti, "Optical frequency conversion in integrated devices," J. Opt. Soc. Am. B **28**(12), A67 (2011).
15. G. P. Agrawal, *Nonlinear Fiber Optics* (Academic, 2001)
16. I. D. Rukhlenko, M. Premaratne, and G. P. Agrawal, "Effective mode area and its optimization in silicon-nanocrystal waveguides," Opt. Lett. **37**(12), 2295–2297 (2012).

#204176 - $15.00 USD Received 7 Jan 2014; revised 24 Jan 2014; accepted 26 Jan 2014; published 27 Feb 2014

17. Y. Shoji, T. Ogasawara, T. Kamei, Y. Sakakibara, S. Suda, K. Kintaka, H. Kawashima, M. Okano, T. Hasama, H. Ishikawa, and M. Mori, "Ultrafast nonlinear effects in hydrogenated amorphous silicon wire waveguide," Opt. Express **18**(6), 5668–5673 (2010).
18. M. Foster, K. Moll, and A. Gaeta, "Optimal waveguide dimensions for nonlinear interactions," Opt. Express **12**(13), 2880–2887 (2004).
19. K. Inoue, H. Oda, N. Ikeda, and K. Asakawa, "Enhanced third-order nonlinear effects in slow-light photonic-crystal slab waveguides of line-defect," Opt. Express **17**(9), 7206–7216 (2009).
20. A. Trita, C. Lacava, P. Minzioni, J. P. Colonna, P. Gautier, J. M. Fedeli, and I. Cristiani, "Ultra-high four wave mixing efficiency in slot waveguides with silicon nanocrystals," Appl. Phys. Lett. **99**(19), 191105 (2011).
21. R. Ahmad and M. Rochette, "High efficiency and ultra broadband optical parametric four-wave mixing in chalcogenide-PMMA hybrid microwires," Opt. Express **20**(9), 9572–9580 (2012).
22. V. Eckhouse, I. Cestier, G. Eisenstein, S. Combrié, P. Colman, A. De Rossi, M. Santagiustina, C. G. Someda, and G. Vadalà, "Highly efficient four wave mixing in GaInP photonic crystal waveguides," Opt. Lett. **35**(9), 1440–1442 (2010).

1. Introduction

The development of optical circuits that integrate several functions on the same chip has been a very active research field during the last two decades. Most of the attention is currently focused on the Silicon-on-insulator (SOI) platform because it provides several advantages, such as a well-developed and mature fabrication technology, the possibility to obtain high refractive-index contrast waveguides, which enable the fabrication of small-footprint components and the integration of optical and electronic circuits on the same substrate [1]. However, as optical material Silicon has two great limitations: its indirect bandgap prevents light amplification by electrical injection, thus hampering the monolithic integration of light sources or amplifiers. In addition, ultrafast nonlinear operations at 1.55 μm are hindered by the insurgence of two-photons-absorption and free-carriers-absorption (TPA and FCA respectively), thus reducing the efficiency of high bit-rate signal processing devices [2].

AlGaAs is an alternative and promising material for the realization of integrated devices. Indeed they were studied since more than ten years as nonlinear devices [3,4]. In recent years, the improvements in waveguide fabrication technology have enabled to precisely tailor the mode distribution and dispersion in waveguides with large nonlinear coefficients and negligible nonlinear absorption at 1.55 μm [5–7]. As a result, many functionalities were demonstrated by means of nonlinear effects in AlGaAs waveguides, such as optical wavelength conversion [6,8], format conversion [7], and phase modulation by exploiting self-phase modulation (SPM) or cross-phase modulation (XPM) [6,9]. Nevertheless, only waveguides with relatively large modal area were generally investigated, thus preventing both nonlinear operation at low power and the possibility to reduce the optical circuit footprint. To address these limitations, photonic nanowires with sub-μm^2 modal cross-sections emerged as a very appealing geometry [9,10]. The superior modal confinement in nanowire geometries makes them ideal for the development of compact-linear devices that can operate at mW-power levels. Up to nowadays, the major drawback of these waveguides has been the very large propagation losses that severely limited their non-linear efficiency [10].

In this paper we report the nonlinear optical characterization of low-loss AlGaAs waveguides over different lengths and cross-sections, with particular emphasis on their nonlinear properties. Thanks to strong optical confinement and low propagation loss we obtained efficient nonlinear behavior with optical power levels as low as a few mW under continuous wave (CW) operation. This is a key result, as it allows for a straightforward analysis of the experimental data, providing reliable and accurate value of the nonlinear coefficients. On the contrary, all the nonlinear experimental results on AlGaAs waveguides reported in the literature use high peak-power laser pulses. Such measurements call for an accurate characterization of the spectral and temporal profile of the input pulses and require a careful numerical analysis of their propagation through the waveguides.

#204176 - $15.00 USD Received 7 Jan 2014; revised 24 Jan 2014; accepted 26 Jan 2014; published 27 Feb 2014

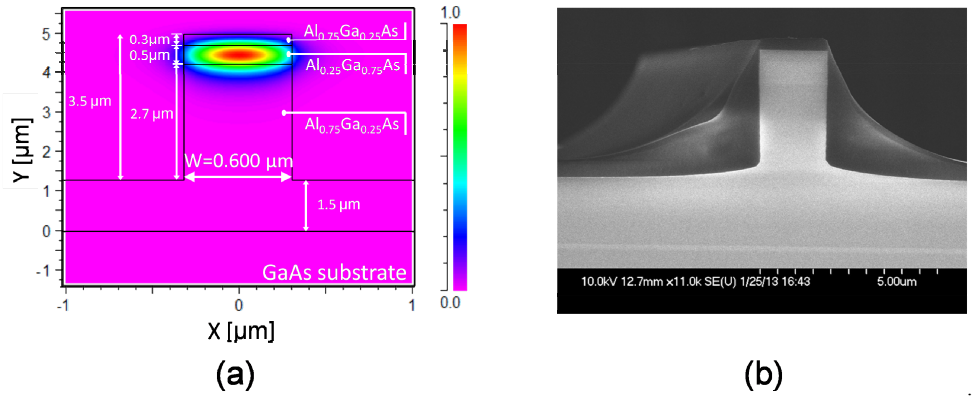

Fig. 1. a) Waveguide cross-section with the layer structure and the modal profile of the fundamental TM mode for a waveguide width w = 0.6 µm. b) Scanning electron microscope image of the cleaved facet.

2. Fabrication

The devices were fabricated in the James Watt Nanofabrication Centre (JWNC) at Glasgow University. The material consisted of a GaAs substrate on which a GaAs/AlGaAs multilayer structure was grown by molecular beam epitaxy (MBE). Starting from the substrate, the layers consisted of a lower cladding of $Al_{0.75}Ga_{0.25}As$, a core layer of $Al_{0.25}Ga_{0.75}As$, an upper cladding of $Al_{0.75}Ga_{0.25}As$ and finally a thin cap layer of GaAs. The thicknesses of the different layers are shown in Fig. 1(a) together with the simulated profile for the TM polarized mode in a waveguide with width w = 0.6 µm. The simulated modal profiles were used to evaluate the effective area A_{eff}. The deeply etched waveguide geometry provides high lateral index-contrast and exhibits single-mode propagation for widths in the range 0.5 to 1.2 µm. The exact molar fraction and energy bandgap of the core layer was verified through photoluminescence measurements using a Fourier Transform Infrared (FTIR) Spectrometer, with obtained values of 0.2565 and 1.7420 eV (0.712 µm), respectively. The corresponding half-bandgap energy is sufficiently shifted to make any residual TPA absorption from band tail states negligible at the operating wavelength of 1.55 µm [4].

The pattern was defined by electron beam lithography (EBL) using hydrogen silsesquioxane (HSQ) as a resist, and it contained several sets of straight waveguides with different lengths (2.5, 3.0 and 3.5 mm) and widths (from 0.6 µm to 1 µm by 0.1 µm steps). Tapers, 150 µm-long, were used on either side of the waveguides to increase coupling efficiency and to facilitate output collection, with the final width of the taper section at the chip facet set to 2 µm. Beam-propagation method (BPM) simulations were used to assess the minimum taper length for adiabatic mode-size conversion [11], and 150 µm was found to be sufficient for avoiding excitation of higher order modes for all considered waveguides widths. Following mask definition through EBL, the structures were etched to a depth of 3.5 µm, a value chosen by means of numerical simulation in order to avoid substrate mode losses. Reactive ion etching (RIE) with a $SiCl_4$-based recipe was used to define the deep-etched structures, being a well-known chemistry, and providing a non-selective and uniform etch of GaAs/AlGaAs multilayer structures with good verticality and sidewall roughness of a few nm [12]. After dry etching, poly-methyl-methacrylate (PMMA, n = 1.481 @ 1.550 µm) was spin-coated on the sample as a protective layer, prior to cleaving of the devices. Figure 1(b) shows a scanning electron microscope (SEM) image of the cleaved facet, where the core layer is clearly visible.

#204176 - $15.00 USD Received 7 Jan 2014; revised 24 Jan 2014; accepted 26 Jan 2014; published 27 Feb 2014

3. Linear characterization

The characterization of propagation and coupling losses was performed on the two sets of waveguides having lengths L_1 = 2.5 mm and L_2 = 3.5 mm, respectively. In waveguides with 0.4 μm and 0.5 μm width, no guided-propagation was observed because both TE and TM polarized modes were below cut-off. As a consequence the measurements were taken on waveguides with a width in the range 0.6-1 μm. Two main sources of losses were considered: propagation losses in the narrow waveguide section (α_0) and coupling losses (α_{coup}), which are due to fiber-to-waveguide coupling losses and propagation losses in the taper-section. The two sets of waveguides, have identical taper sections but different lengths, in particular $\Delta L = L_2 - L_1 = 1$ mm. Hence we were able to isolate the propagation loss contribution by measuring the transmission through both sets of waveguides. The difference in transmission has to be ascribed to the propagation in a section of waveguide with length ΔL, from which the α_0 coefficient can be extracted. Coupling losses were then determined by subtracting the propagation losses from the overall waveguide insertion loss.

The optical source used for the measurements was a tunable laser spanning the wavelength range 1.53-1.56 μm. To select a linear state of polarization the source was connected to a polarization beam splitter (PBS). One of the PBS fiber output was then spliced to a polarization-maintaining (PM) tapered fiber. The output beam of the tapered fiber had a mode field diameter of 2.5 μm. The power was monitored by a power-meter placed before the PBS, and an all-fiber polarization controller was used to maximize the power in the selected state of polarization. The tapered PM fiber was inserted in a precision mountable to rotate with respect to its longitudinal axis. TE and TM polarization states could be then selectively launched into the waveguides by rotating the principal axes of the input PM fiber by 90°. Propagation losses were similar for both the TE and TM mode and ranged from 4 to 5 dB/cm for the 1 μm wide waveguide to 6-7 dB/cm for the 0.7 μm waveguide. For the smallest cross section waveguide (w = 0.6 μm), a sharp increase in the propagation loss for the TE mode was measured (i.e. 17 dB/cm loss compared to the 6.5 dB/cm of the TM mode). This result can be explained considering that for a waveguide width of 0.6 μm the TE mode is very close to cut-off. Hence, the assessment of CW nonlinear optical performance on the 0.6 μm-wide waveguide for which the FWM efficiency was highest was performed considering the TM mode only.

The loss measurements showed that, as expected, higher propagation losses occur for smaller waveguide cross sections, in which the interaction of the mode with the etched interfaces is more relevant (see Fig. 2) [13]. The coupling losses are about 8.5 dB that is one of the best values reported for this kind of waveguides.

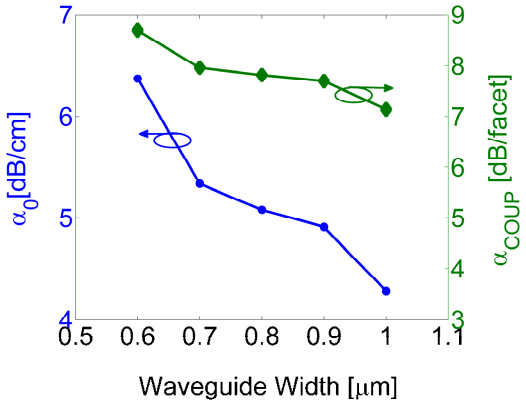

Fig. 2. Propagation loss as a function of waveguide width (blue circles) and coupling loss as a function of waveguide width (green diamonds).

#204176 - $15.00 USD Received 7 Jan 2014; revised 24 Jan 2014; accepted 26 Jan 2014; published 27 Feb 2014

4. Nonlinear characterization

The main goal of this work was the assessment of the real part of the γ coefficient by means of CW four-wave mixing (FWM) experiments. Figure 3 shows the experimental setup, where an intense CW pump beam and a weaker CW probe (wavelength tunable) were polarization controlled, combined by a 90/10 (pump/signal) fiber coupler, and then input to a PBS, so as to guarantee that the light input to the waveguide was TM-polarized. The wavelength of signal and pump were kept very close ($\Delta\lambda$ < 1nm) to make negligible the phase mismatch in the nonlinear interaction.

The output radiation was collected by a tapered single mode fiber, connected to an Optical Spectrum Analyzer (OSA), to enable the independent measurement of the power carried by the probe beam and idler beam at the waveguide output. FWM efficiency was calculated as the ratio between idler-power and probe-power using the following expression:

$$\frac{P_{idler}(L)}{P_{probe}(L)} = \left(\eta P_{pump}(0) L_{eff} \operatorname{Re}(\gamma)\right)^2. \quad (1)$$

where $\eta = 1$ when the phase matching condition is satisfied.

The obtained values for the Re(γ) are shown in Fig. 4, as a function of the waveguide width.

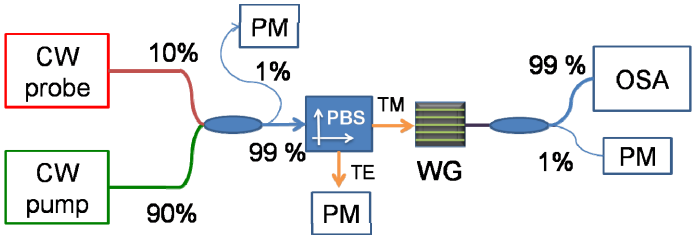

Fig. 3. Schematic of the experimental FWM-setup. PM: Power Meter; PBS: Polarization Beam Splitter; OSA: Optical Spectrum Analyzer.

As expected, smaller waveguides exhibit a higher nonlinear coefficient due to the stronger optical mode confinement. For the 0.6 μm-wide waveguide we obtain a nonlinear parameter Re(γ) ≈521 $W^{-1}m^{-1}$, which is the highest figure reported in the literature for waveguides based on this material [6,8,14]. We also evaluated the nonlinear refractive index n_2 for the different waveguides, by combining the experimental values of Re(γ) with the effective area values by using the expression $\operatorname{Re}(\gamma) = (2\pi n_2)/(\lambda A_{eff})$ [15]. A_{eff} values were calculated by using the following equation [16]:

$$A_{eff} = \frac{a_{NL}\int_{-\infty}^{\infty}\int S_z dxdy}{\iint_{NL} S_z dxdy}. \quad (2)$$

where $S_z = (\mathbf{E}\times\mathbf{H})\cdot z$ is the time averaged z component of the Poynting vector, z is the unit vector along the waveguide axis, a_{NL} is the core cross section area and NL denotes the integration over the nonlinear region. Electric and magnetic field distributions were evaluated by means of numerical simulations carried out with Rsoft Beamprop. Equation (2) allows evaluating A_{eff} in strongly confined structures. It is worth noting that, for such waveguides, the value of A_{eff} could significantly differ from a_{NL} when the waveguide cross-section sizes are much smaller than the operating wavelength (see Fig. 4 inset) [16–18].

The results, reported in Fig. 4 (green line), confirm that the measured n_2 values (1.98 ± 0.5 x 10^{-17} m^2/W) are in good agreement with the typical figures reported in the scientific literature [5,8].

#204176 - $15.00 USD Received 7 Jan 2014; revised 24 Jan 2014; accepted 26 Jan 2014; published 27 Feb 2014

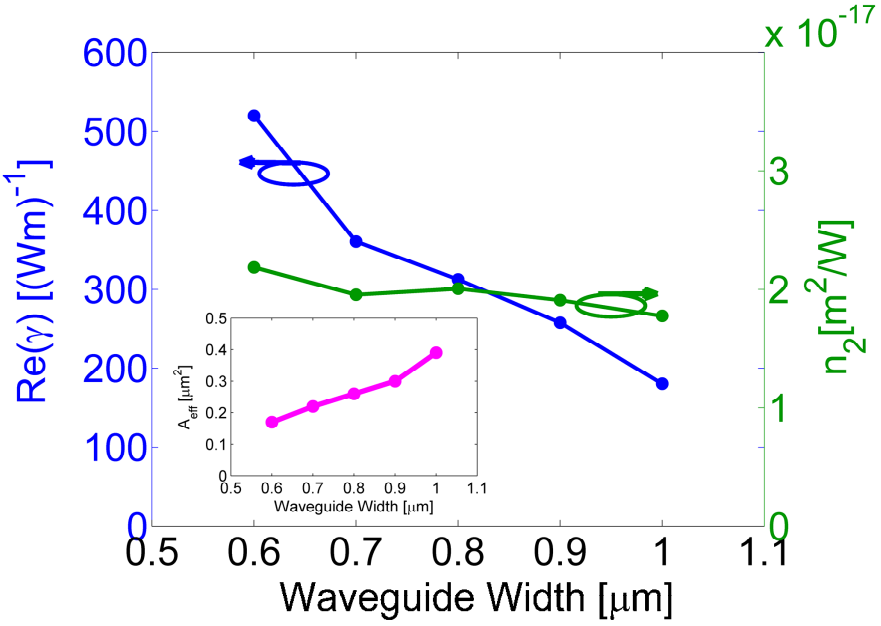

Fig. 4. Real part of gamma (blue line) and estimated n_2 (green line) as a function of the waveguide width. Inset: A_{eff} as a function of the waveguide width calculated by numerical simulations.

In a second set of experiments we measured the FWM efficiency as a function of the input pump power, in order to evaluate the presence of nonlinear absorption. The results, shown in Fig. 5 for the 0.6 μm-wide waveguide, indicate that the FWM efficiency increases quadratically with the pump power with no saturation, even when high-intensity beams (e.g. 7 MW cm^{-2}) propagate in the waveguide. The experimental data can be fitted by a parabolic curve, as described by Eq. (1). Setting in the fit the experimental value of L_{eff} we obtain Re(γ) = 521 W^{-1}m^{-1} as reported in the inset of Fig. 5(a)

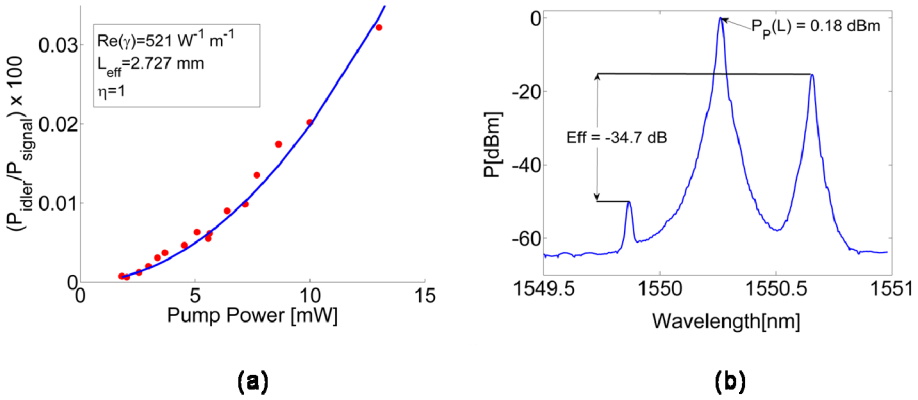

Fig. 5. a) FWM efficiency as a function of the pump power for a 3.5 mm long waveguide with w = 0.6 μm; red circles represent the experimental data while the blue line is the fitting function obtained by using the parameters indicated in the inset. b) Experimental spectra recorded at the output of the same waveguide with a coupled pump power of 13 mW.

#204176 - $15.00 USD Received 7 Jan 2014; revised 24 Jan 2014; accepted 26 Jan 2014; published 27 Feb 2014

A FWM efficiency of −34.7 dB (see Fig. 5(b)) was measured in the CW regime with a coupled pump power of 13 mW. Equation (1) clearly shows that the absolute value of the FWM efficiency can be enhanced by increasing the pump power value at the AlGaAs waveguide input. However, due to the coupling loss of our waveguides the maximum available input pump power in our experiments, estimated after the tapering section, was about 13 mW thus preventing higher FWM efficiency values.

In order to compare the nonlinear performance of different waveguides, it is useful to introduce a suitable figure of merit (FOM). In the literature the following FOM is often considered [15,19], which provides the total phase shift per unit power that is cumulated by a signal due to the contribution of the nonlinear refractive index.

$$\eta_1 = \gamma L_{eff}. \tag{3}$$

Nevertheless, when dealing with integrated optical circuits, the waveguide footprint becomes a critical issue. Hence it is worth considering a different FOM [20] in which the FWM nonlinear efficiency is normalized with respect to both the waveguide length and the pump power:

$$\eta_2 = \frac{100 \times P_{idler} / P_{probe}}{P^2_{pump} L^2}. \tag{4}$$

Table 1 reports η_1 and η_2 calculated for the available data obtained in AlGaAs waveguides. For a comparison we report also the values obtained with the most efficient waveguides reported in the literature fabricated on different platforms.

It can be noticed that the values of η_1 and η_2 obtained in this work for the 0.6 μm wide waveguide is considerably higher than the data reported in the literature for other AlGaAs waveguides. Chalcogenide nanowires provide a much better value of η_1 [21] but, as expected, the value of η_2 highlights that these waveguides are not suitable for integration in miniaturized optical circuits. Moreover, it is worth noting that similar efficiency values have been previously obtained in resonant structures such as photonic-crystal GaInP waveguides [22], which are inherently narrow-band devices or in Si-based slot-waveguides [20]. In the latter, the nonlinearity was enhanced by the presence of silicon nanocrystals and high power operation was still hindered by TPA and FCA.

Table 1. Performance comparison between different nonlinear semiconductor waveguides

Waveguide	Re(γ) [$W^{-1}m^{-1}$]	η_1	η_2 [$W^{-2}mm^{-2}$]
AlGaAs [8]	10	0.09	10^{-7}%
AlGaAs [10]	20	0.07	not measured
AlGaAs [6]	68	1.03	0.11%
Present Work	521	1.39	14%
GaInP [22]	2900	2.11	23.8%
As_2S_3 –nanowire [21]	63	6.19	1.1%
Si - Si:nc [20]	1100	4.43	112.2%

5. Conclusion

In this work we experimentally report on the non-linear characterization of AlGaAs optical nanowires. We measured, in a CW regime, the real part of their nonlinear coefficient and analyzed its dependence on waveguide cross-section. We obtained the highest value ever reported for AlGaAs waveguides of Re(γ) = 521 $W^{-1}m^{-1}$. Furthermore a normalized efficiency equal to 14% $W^{-2}mm^{-2}$ is demonstrated, and TPA is found to be negligible in the range of investigated operating powers.

#204176 - $15.00 USD Received 7 Jan 2014; revised 24 Jan 2014; accepted 26 Jan 2014; published 27 Feb 2014

We believe that AlGaAs can represent a viable choice for stand-alone nonlinear optical based devices. In addition it could be the ideal material to functionalize silicon photonic integrated devices as well, by replacing silicon when high power propagation is required.

Acknowledgments

The authors acknowledge the support from the technical staff of the James Watt Nanofabrication Centre at Glasgow University and V.P. acknowledges partial financial support from the GRPE programme and EPSRC under grant agreement EP/P504937/1.

#204176 - $15.00 USD Received 7 Jan 2014; revised 24 Jan 2014; accepted 26 Jan 2014; published 27 Feb 2014